ISSN 2616-5767 Vol.8, Issue 5: 10-18, DOI: 10.25236/AJETS.2025.080502

Dynamic Design and Active Control of Piezoelectric Phononic Crystal Beams for Vibration Suppression

Hanbo Shao*, Xiaochen Hang, Weiyu Chen

School of Mechanical and Electronic Engineering, Nanjing Forestry University, Nanjing, 210037, Jiangsu, China

Abstract: *This study theoretically and numerically explores a dynamic design to control elastic wave actively in a piezoelectric phononic crystal beam using tunable LRC shunt circuits. Based on piezoelectric constitutive equations and electromagnetic resonance principles, the equivalent elastic modulus of the piezoelectric patches is derived as a circuit-dependent complex parameter. By systematically adjusting resistance, inductance, and capacitance, the position and attenuation strength of the electromagnetic oscillation bandgap (EOBG) can be effectively tuned. Results indicate that variations in R alter only the transmission loss without affecting the bandgap frequency. In contrast, increasing L or C reduces the bandgap frequency, while simultaneously enhancing wave energy dissipation through intensified electromagnetic oscillation. Reducing R, increasing L, or decreasing C amplifies the magnitude and phase angle of the equivalent modulus, leading to improved vibration attenuation within the bandgap. The study demonstrates that real-time tuning of LRC circuits enables precise and adaptive control over wave propagation, offering a practical strategy for designing smart metamaterials with customized wave manipulation and vibration suppression capabilities.*

Keywords: *Phononic Crystal, Piezoelectric Patch, Bandgap, Vibration Suppression*

1. Introduction

In recent years, the study of elastic wave control through acoustic metamaterials [1–2] or periodic structure like phononic crystals [3–5] has become a highly active research area. Phononic crystals exhibit specific acoustic passbands and stopbands within certain frequency ranges [6–9]. Passbands allow waves to propagate through the structure with minimal energy loss. This characteristic is utilized in the design of acoustic devices such as filters and waveguides [10–13]. In contrast, stopbands prevent wave propagation at corresponding frequencies, a phenomenon that has been analyzed in detail in preceding sections. Many researchers have exploited this feature to develop novel materials with functionalities such as acoustic black holes, multifunctional filters, and acoustic diodes [14–15]. People [1,16] investigated elastic metamaterials made up of solid constituents and observed the emergence of stopbands in adjustable frequencies accompanied by negative effective mass density. Liu [17] removed one or more cylindrical inclusions to introduce point and line defects in sandwich plates, and employed the finite element method to study Lamb wave propagation in these structures. Yang [18] designed an elastic metamaterials structure with membrane component and demonstrated existence of stopbands within the 200–300 Hz range, confirming their presence even at low frequencies. By varying the radius of the defective cylinders, wave localization was achieved near the defect region without leakage into the surrounding medium. Furthermore, the removal of an entire row of cylinders to form a line defect allowed guided wave modes to emerge within the stopband. This approach offers a novel strategy for controlling wave propagation or isolating vibrations at specific frequencies, with potential applications in defect detection and waveguide design. In summary, acoustic metamaterials enable precise control over wave propagation within selected frequency ranges and demonstrated perfect physical performance in the past two decades. However, some acoustic metamaterials and phononic crystals like passive structure suffer from limitations such as narrow bandwidth, single-frequency operation, and lack of adaptability, which restrict their practical applicability.

With the development of piezoelectric and electromagnetic technologies and the wide application of piezoelectric smart materials [19–20], Lots of researchers have begun integrating piezoelectric components into phononic crystals to overcome the limitations of passive elastic metamaterials. Akl and his team [21–22] investigated active tuning techniques for wave control in acoustic metamaterials and designed a periodic structure with tunable effective density. The structure is made up of some liquid

ISSN 2616-5767 Vol.8, Issue 5: 10-18, DOI: 10.25236/AJETS.2025.080502

cavities divided by piezoelectric diaphragms. The vibrational state of the diaphragms and the effective parameters of the metamaterial can be controlled via external voltage, thereby enabling modulation of acoustic transmission in target frequency bands [23]. Such a configuration allows the adjustment of acoustic transmission across different frequencies without altering the physical structure, significantly expand its potential for practical application. Cummer and his team [24] developed an actively tunable acoustic metamaterial for cloaking applications. Embedded piezoelectric sensors within the structure measure incident pressure waves, and after processing by internal circuits, electrical signals drive piezoelectric diaphragms to regenerate the transmitted wave. Their experimental results confirmed that without changing the structures, this function can be tuned in real time. Thereby demonstrating active control over acoustic waves. Thus, piezoelectric technology provides a promising avenue for actively controlling wave propagation in metamaterials and offers significant advantages in vibration and noise reduction research.

Nevertheless, current piezoelectric control techniques primarily focus on adjusting frequency ranges or modifying the width of passbands and stopbands. There remains limited research on the spatial control of wave transmission. This paper presents a numerical analysis of elastic wave in one-dimensional beam-type piezoelectric phononic crystals, aiming to further investigate the active control of elastic waves through piezoelectric effects. The main contributions of this study include:

(1) Deriving the relationship among the natural frequency, phase angle under electromagnetic resonance, and the LCR circuit parameters, and achieving the transformation between mechanical and electrical energy via positive piezoelectric effect.

(2) Designing a one-dimensional beam-structured piezoelectric phononic crystal, utilizing piezoelectric shunt technology for active control of wave propagation, and demonstrating the structural feasibility through numerical simulations.

(3) Investigating the influence of resistance R, inductance L, and capacitance C on electromagnetic oscillation effects, clarifying the mechanism of transmission loss variation at the natural frequency of EOBG, and studying the attenuation process of vibration propagation in the piezoelectric acoustic metamaterial.

(4) Demonstrating the feasibility of actively controlling the position and transmission loss of the elastic wave bandgap by adjusting the LCR circuit, thereby enhancing the overall vibration damping performance of the structure.

2. Model and theory

This section employs the piezoelectric shunt technique to achieve active control of wave propagation, facilitating the transformation between mechanical and electrical energy through direct piezoelectric effect. Figure 1 illustrates the schematic configuration of the beam-type piezoelectric phononic crystal. By periodically bonding piezoelectric patches onto a homogeneous beam, the physical parameters of the structure are modulated periodically, thereby altering the position and width of the phononic bandgap and enabling active acoustic wave control.

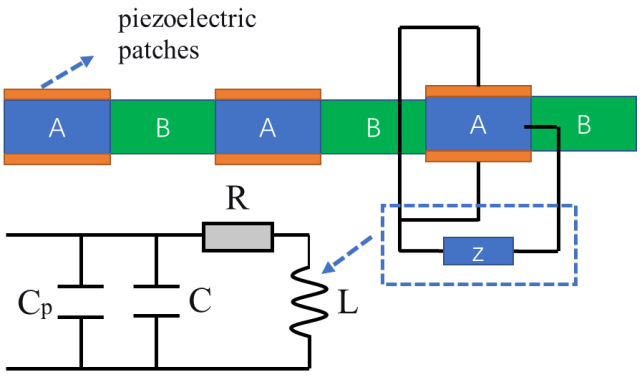

Figure 1 Structural Model of a One-Dimensional Beam-Type Piezoelectric Phononic Crystal and Simplified Diagram of the LCR Circuit

In Figure 1, the substrate beam is made of epoxy resin. The unit cell is consists of two parts, A and B. In part A, piezoelectric ceramic patches (made of PZT-5H) are periodically attached on both surfaces.

ISSN 2616-5767 Vol.8, Issue 5: 10-18, DOI: 10.25236/AJETS.2025.080502

The height and length of each piezoelectric patch are denoted as *d* and *l*, respectively. The piezoelectric shunt circuit Z, consists of a resistor, a capacitor, an inductor — commonly referred to as an LCR circuit, the capacitance of each piezoelectric patch is represent as C_p.

Assuming that all piezoelectric patches along the length direction are under free boundary conditions on the surfaces (except for the inner interface) and are only influenced by the electric field along the thickness direction, the piezoelectric constitutive equations can be simplified as follows [25]:

$$S_1 = s_{11}^E T_1 + d_{31} E_3 \qquad D_3 = d_{31} T_1 + \varepsilon_{33}^T E_3 \tag{1}$$

Where T_1, S_1, D_3 and E_3 represent the stress, strain, electric displacement and electric field strength of each piezoelectric patch, respectively; ε_{11}^E, ε_{33}^T and d_{31} is the elastic compliance constant, the free dielectric constant and the piezoelectric strain constant, respectively.

In Figure 1, the electrical resistance of the epoxy resin can be neglected, so the fundamental circuit equation is expressed as [26]:

$$I = \frac{U}{Z} = \frac{E_3 h_p}{Z}, \quad I = -A_s D_3 S \tag{2}$$

Where U, h_p, A_s and Z is electric potential difference, the thickness and the area of the patches, the combined impedance of the LCR circuit, respectively, which can be expressed by the following formula:

$$Z = \frac{R + Ls}{1 + RCs + LCs^2} \tag{3}$$

From Equations (1) and (2), it can be got as follow:

$$S_1 = \left(s_{11}^E - \frac{s Z d_{31}^2 A_s h_p^{-1}}{1 + s Z C_p} \right) T_1 \tag{4}$$

Where C_p is intrinsic capacitance:

$$C_p = \frac{\varepsilon_{33}^T A_s}{h_p} \tag{5}$$

According to Equation (4), we can express the equivalent elastic modulus of the piezoelectric patch as:

$$E_p = \frac{T_1}{S_1} = \frac{h_p \left(1 + s Z C_p\right)}{h_p s_{11}^E \left(1 + s Z C_p\right) - s Z d_{31}^2 A_s} \tag{6}$$

At this point, by setting $s = i\omega$ and combining Equations (3) and (6), the equivalent elastic modulus of the piezoelectric patch can be expressed as follows:

$$E_p = \frac{1 - L\left(C + C_p\right)\omega^2 + \omega R\left(C + C_p\right) i}{s_{11}^E - L\left[s_{11}^E \left(C + C_p\right) - d_{31}^2 A_s h_p^{-1} \right]\omega^2 + \omega R\left[\left(C + C_p\right) s_{11}^E - d_{31}^2 A_s h_p^{-1} \right] i} \tag{7}$$

Using the following formula for the natural frequency under electromagnetic resonance:

$$f = \frac{1}{2\pi \sqrt{L\left(C + C_P\right)}} \quad \omega = 2\pi f \tag{8}$$

Where C is the capacitance connected in the circuit, and C_p is the intrinsic capacitance of the piezoelectric patch. As indicated by Equation(7), $|E_p|$ is the magnitude of the equivalent elastic modulus of the piezoelectric patch , and its phase angle can be expressed as:

ISSN 2616-5767 Vol.8, Issue 5: 10-18, DOI: 10.25236/AJETS.2025.080502

$$Arg\left(E_p\right)=\arctan\left(\frac{m}{n}\right) \tag{9}$$

Where:

$$\begin{aligned} m &= \omega R\left(C+C_p\right)\cdot\left(s_{11}^E-L\left[s_{11}^E\left(C+C_p\right)-d_{31}^2A_sh_p^{-1}\right]\omega^2\right) \\ &-\left[1-L\left(C+C_p\right)\omega^2\right]\cdot\left(\omega R\left[\left(C+C_p\right)s_{11}^E-d_{31}^2A_sh_p^{-1}\right]\right) \\ &= \omega R d_{31}^2A_sh_p^{-1} \\ n &= \left[1-L\left(C+C_p\right)\omega^2\right]\cdot\left(s_{11}^E-L\left[s_{11}^E\left(C+C_p\right)-d_{31}^2A_sh_p^{-1}\right]\omega^2\right) \\ &+\omega R\left[\left(C+C_p\right)s_{11}^E-d_{31}^2A_sh_p^{-1}\right] \end{aligned} \tag{10}$$

3. Simulation

In photonic crystals, electromagnetic waves can propagate through air or vacuum [27], resulting in some energy to radiate into the surrounding air rather than being confined within the defect state. Therefore, when evaluating the localization of light waves in defective photonic crystal slabs, it is necessary to account for the dielectric media both above and below the slab. In contrast, for phononic crystals, acoustic waves are generally considered to be entirely confined within the structure. As a result, the coupling between structural vibrations and airborne sound can be neglected. Compared to photonic crystals, the design and analysis of phononic crystals do not require consideration of air-related cutoff effects.

The one-dimensional beam-type piezoelectric phononic crystal is composed of an epoxy resin substrate and piezoelectric patches. The physical parameters of the simulation model are listed in Table 1, and the geometric parameters are as follows: the height of the beam is h = 5 mm; the length of part A in the unit cell is a = 40 mm; part B is b = 40 mm; the piezoelectric patch is c = 20 mm; and its height is h_p = 0.5 mm.

Table 1 Parameters of the one-dimensional beam-type piezoelectric phononic crystal.

Materials	Elastic Modulus (GPa)	Poisson's Ratio	Density (kg/m^3)	
Epoxy Resin	210.600	0.5	1180	
Piezoelectric Patch	Compliance Constant (m^2/N)	Piezoelectric Constant (C/m^2)	Dielectric Constant (F/m)	Density (kg/m^3)
	1.65×10^{-11}	-2.74×10^{-10}	3.01×10^{-8}	7500

3.1 Influence of resistance on the EOBG and equivalent modulus

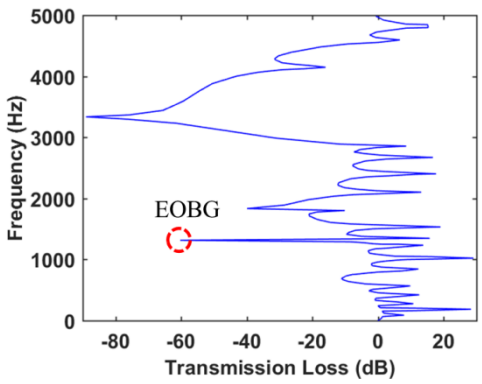

Figure 2 Transmission curve of the piezoelectric phononic crystal when R = 0.

ISSN 2616-5767 Vol.8, Issue 5: 10-18, DOI: 10.25236/AJETS.2025.080502

With the inductance L=50mH and capacitance $C=2\times10^{-7}$ F in the LCR circuit held constant, and the resistance set to R = 0, the central frequency of the EOBG is given by Equation (8). As shown in the transmission curve in Figure 2, two intrinsic bandgaps are observed at 1800 Hz and 3300 Hz. These bandgaps are independent of the LCR circuit and are referred to as the first and second intrinsic bandgaps, respectively. Additionally, an EOBG appears at 1428 Hz, which is determined by the piezoelectric patches and the LCR circuit. It can be seen that when R = 0, the EOBG is clearly defined, and its transmission loss is significantly greater than that of the first intrinsic bandgap but less than that of the second intrinsic bandgap.

Based on the determined position of the EOBG, the resistance value in the circuit was varied. Figure 3(a), (b), and (c) show the transmission curves when R = 0 Ω, 100 Ω, and 500 Ω, respectively. As the resistance increases, the current in the LCR circuit decreases, leading to a reduction in the voltage across the piezoelectric patches. As a result, the direct piezoelectric effect becomes less pronounced, causing a significant decrease in the transmission loss of the EOBG. When R = 500 Ω, the EOBG nearly disappears.

Figure 4(a) and (b) illustrate the variation in the magnitude and phase angle of the equivalent elastic modulus E_P by changing the resistance of piezoelectric patch. It can be clearly observed that as the resistance decreases, the magnitude of E_P increases, indicating more significant electromagnetic oscillation effects. Correspondingly, the phase angle also increases under these conditions.

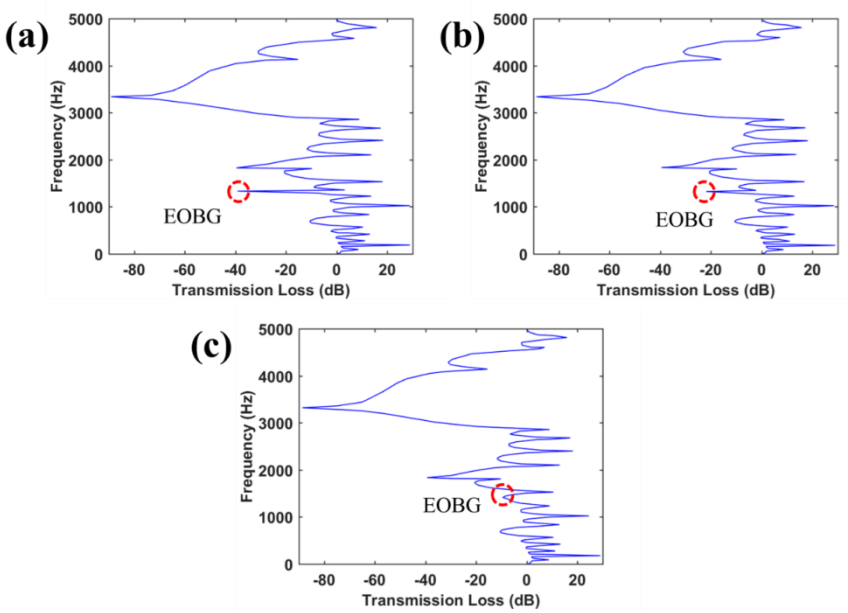

Figure 3 Transmission curves of the piezoelectric phononic crystal under different resistance values: (a) R = 0 Ω, (b) R = 100 Ω, (c) R = 500 Ω.

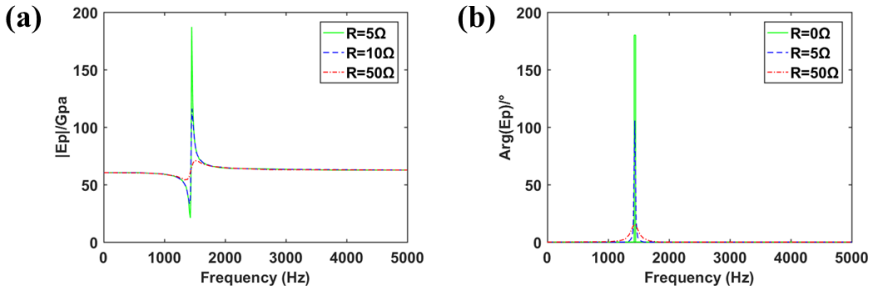

Figure 4 (a) Variation of the E_P of the piezoelectric patch with resistance; (b) Variation of the phase angle with resistance

3.2 Influence of inductance on the EOBG and equivalent modulus

Building on the previous subsection, with the resistance R and capacitance C R=5Ω，$C=2\times10^{-7}F$

ISSN 2616-5767 Vol.8, Issue 5: 10-18, DOI: 10.25236/AJETS.2025.080502

held constant, the inductance value was varied. Figure 5 shows the transmission curves for inductance values of L=10、20、50mH , respectively.

When L=10mH , the central frequency of the EOBG is calculated from Equation (8) as f = 3195Hz . As shown in Figure 5(a), the EOBG coincides with the second intrinsic bandgap of the acoustic metamaterial. Since the transmission loss of the electromagnetic bandgap is relatively small compared to that of the second intrinsic bandgap, the influence of the LCR circuit on the phononic crystal is minimal in this case. When L=20mH , the calculated central frequency is f = 2259Hz . Figure 5(b) shows that an EOBG appears between the first and second intrinsic bandgaps. Both theoretical and simulation results verify that as the inductance increases, the frequency of the EOBG decreases. When L=50mH , the central frequency is further reduced to f =1428Hz . Figure 5(c) indicates that the EOBG frequency decreases again. Moreover, due to the increased inductance, the current in the circuit strengthens, leading to a more pronounced electromagnetic oscillation effect. Consequently, the transmission loss at the electromagnetic resonance frequency also increases.

Figure 6(a) and (b) illustrate the variations in the magnitude and phase angle of the equivalent elastic modulus E_P by changing the inductance of piezoelectric patch. It can be clearly observed that as the inductance increases, the magnitude of E_P rises, indicating enhanced electromagnetic oscillation effects. Correspondingly, the phase angle also increases under these conditions.

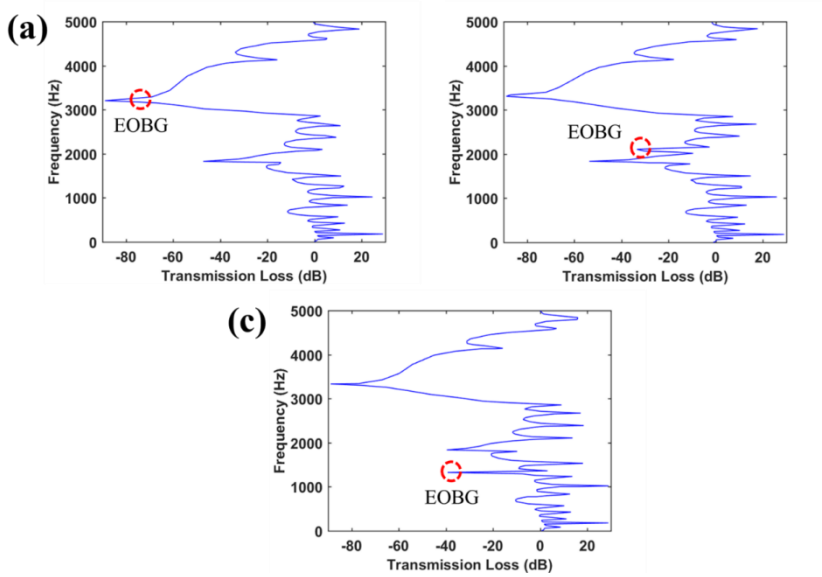

Figure 5 Transmission curves of the piezoelectric phononic crystal under different inductance values: (a) L=10mH *,(b)* L=20mH *,(c)* L=50mH

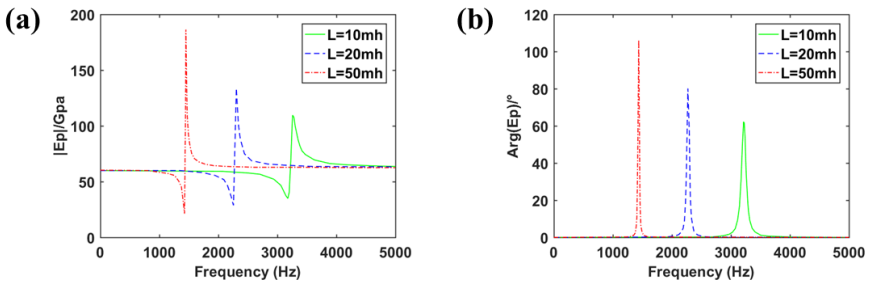

Figure 6 (a) Variation of the E_P *of the piezoelectric patch with inductance; (b) Variation of the phase angle with inductance*

3.3 Influence of capacitance on the EOBG and equivalent modulus

To investigate the effect of capacitance C on the EOBG and the equivalent modulus, the resistance R and inductance L were held constant as R=5Ω，L=50mH while the capacitance value was varied.

ISSN 2616-5767 Vol.8, Issue 5: 10-18, DOI: 10.25236/AJETS.2025.080502

Figure 7 shows the transmission curves for capacitance values of C=10^{-7}, 2×10^{-7}, $5\times10^{-7}F$, respectively.

When C=$10^{-7}F$, the central frequency of the EOBG is calculated from Equation (8) as f =1849Hz .As shown in Figure 7(a), the EOBG coincides with the first intrinsic bandgap of the phononic crystal, resulting in a narrow EOBG within the first intrinsic bandgap. When C=2×10^{-7} F, the calculated central frequency is f =1428Hz. Figure 7(b) shows that an EOBG appears between the first and second intrinsic bandgaps. As the capacitance increases, the frequency of the EOBG decreases. When C=5×10^{-7} F, the central frequency is further reduced to f =961Hz. Figure 7(c) indicates that the EOBG frequency decreases again. Moreover, due to the increased capacitance, the current in the circuit weakens, leading to a diminished electromagnetic oscillation effect. Consequently, the transmission loss at the electromagnetic resonance frequency also decreases, and as can be observed in the figure, the transmission loss at the bandgap nearly disappears.

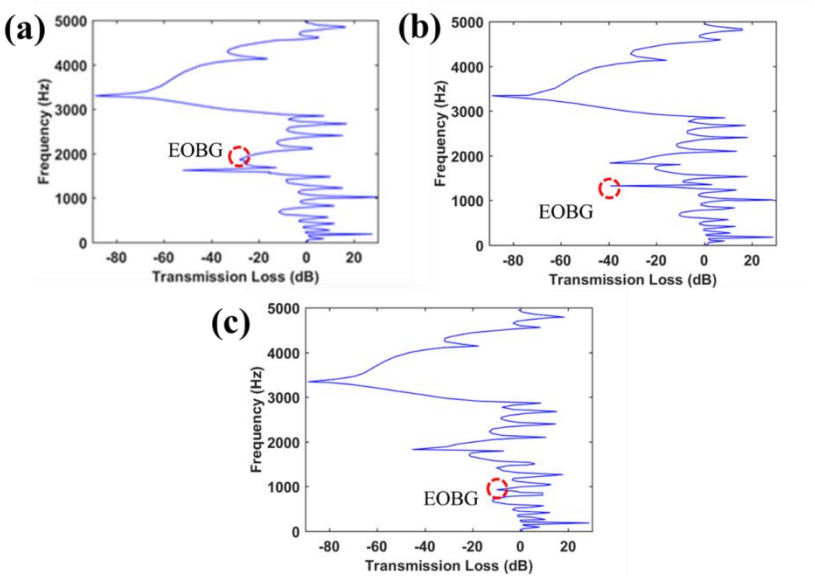

Figure 7 Transmission curves of the piezoelectric phononic crystal under different capacitance values: (a) C=10^{-7} F *,(b)* C=2×10^{-7} F *,(c)* C=5×10^{-7} F.

Figure 8(a) and (b) illustrate the variations in the magnitude and phase angle of the equivalent elastic modulus E_p by changing the capacitance of piezoelectric patch. It can be easily showed that as the capacitance increases, the magnitude of E_p decreases, indicating a gradual attenuation of the electromagnetic oscillation. Correspondingly, the phase angle also decreases under these conditions.

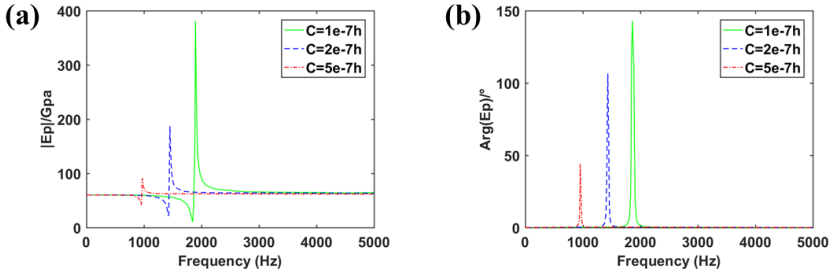

Figure 8 (a) Variation of the E_p *of the piezoelectric patch with capacitance; (b) Variation of the phase angle with capacitance.*

4. Conclusion

This paper investigates the factors influencing the EOBG in a one-dimensional piezoelectric phononic crystal by adjusting parameters of the LRC circuit. The results demonstrate that active control of elastic

ISSN 2616-5767 Vol.8, Issue 5: 10-18, DOI: 10.25236/AJETS.2025.080502

waves can be achieved through regulation of the LRC circuit. The main conclusions include:

(1) Variations in the resistance R do not alter the position of the EOBG but only affect the magnitude of the transmission loss. In contrast, changes in the inductance L or capacitance C not only shift the position of the bandgap but also modify the transmission loss. Specifically, as L or C increases, the oscillation bandgap shifts toward lower frequencies.

(2) A decrease in R, an increase in L, or a decrease in C enhances the electromagnetic oscillation effect. This leads to an increase in the transmission loss at the natrual frequency of the bandgap, thereby strengthening the attenuation of vibration propagation within the piezoelectric acoustic metamaterial and improving the vibration damping performance.

(3) Active control over both the position and transmission loss of the EOBG for elastic waves can be effectively achieved by tuning the LRC circuit parameters.

Acknowledgments

This work was supported by Funding from Natural Science of Jiangsu Province (Grant No. BK20240658).

References

[1] Sheng P, Zhang X X, Liu Z, et al. Locally resonant sonic materials[J]. Science, 2000, 338(1):201-205.
[2] Mei J, Ma G, Yang M, et al. Dynamic Mass Density and Acoustic Metamaterials[J]. Physica B Physics of Condensed Matter, 2007, 394(2):256-261.
[3] Wang Y F, Wang Y S, Laude V. Wave propagation in two-dimensional viscoelastic metamaterials[J]. Physical Review B, 2015, 92(10).
[4] Mei J, Liu Z, Wen W, et al. Effective dynamic mass density of composites[J]. Physical Review B Condensed Matter, 2007, 76(13):134205.
[5] Charles C, Bonello B, Ganot F. Propagation of guided elastic waves in 2D phononic crystals [J]. Ultrasonics, 2006, 44(4):1209.
[6] Liu S, Li S, Shu H, et al. Research on the elastic wave band gaps of curved beam of phononic crystals[J]. Physica B Physics of Condensed Matter, 2015, 457(457):82-91.
[7] Taniker S, Yilmaz C. Phononic gaps induced by inertial amplification in BCC and FCC lattices[J]. Physics Letters Section A General Atomic & Solid State Physics, 2013, 377(31–33):1930-1936.
[8] Han L, Zhang Y, Ni Z Q, et al. A modified transfer matrix method for the study of the bending vibration band structure in phononic crystal Euler beams[J]. Physica B Physics of Condensed Matter, 2012, 407 (23): 4579-4583.
[9] Mei J, Ma G, Yang M, et al. Dark acoustic metamaterials as super absorbers for low-frequency sound[J]. Nature Communications, 2012, 3(2):756.
[10] Lu K, Wu J H, Guan D, et al. A lightweight low-frequency sound insulation membrane-type acoustic metamaterial[J]. Aip Advances, 2016, 6(2):1373.
[11] Tanaka Y, Tamura S I. Surface acoustic waves in two-dimensional periodic elastic structures[J]. Physical Review B, 1998, 58(12):7958-7965.
[12] Hua L, Wang G X, Liu X M. Manipulation of light in MIM plasmonic waveguide systems[J]. Chinese Science Bulletin, 2013, 58(30):3607-3616.
[13] Zhang X J, Guo C J. Cubature Kalman filters: Derivation and extension[J]. Chinese Physics B, 2013, 22(12):497-502.
[14] Shelby R A, Smith D R, Schultz S. Experimental Verification of a Negative Index of Refraction[J]. Science, 2001, 292(5514):77.
[15] Sukhovich A, Merheb B, Muralidharan K, et al. Experimental and theoretical evidence for subwavelength imaging in phononic crystals [J]. Physical Review Letters, 2009, 102(15):154301.
[16] Zhang S, Yin L, Fang N. Focusing ultrasound with an acoustic metamaterial network[J]. Physical Review Letters, 2009, 102(19):194301.
[17] Liu X F, Wang Y F, Wang Y S, et al. Wave propagation in a sandwich plate with a periodic composite core[J]. Journal of Sandwich Structures & Materials, 2014, 16(3):319-338.
[18] Yang Z, Mei J, Yang M, et al. Membrane-type acoustic metamaterial with negative dynamic mass[J]. Physical Review Letters, 2010, 101(20):204301.
[19] Thorp O, Ruzzene M, Baz A. Attenuation of wave propagation in fluid-loaded shells with periodic

ISSN 2616-5767 Vol.8, Issue 5: 10-18, DOI: 10.25236/AJETS.2025.080502

shunted piezoelectric rings[J]. Smart Materials & Structures, 2005, 14(4):594.
[20] Tang J, Wang K W. Vibration Control of Rotationally Periodic Structures Using Passive Piezoelectric Shunt Networks and Active Compensation[J]. Journal of Vibration & Acoustics, 1999, 121(3):379-390.
[21] Baz A M. Active control of a two-dimensional periodic structure[J]. Proceedings of SPIE - The International Society for Optical Engineering, 2004, 53:86.
[22] Akl W, Baz A. Multi-cell Active Acoustic Metamaterial with Programmable Bulk Modulus[J]. Journal of Intelligent Material Systems & Structures, 2010, 21(5):541-556.
[23] Baz A. The structure of an active acoustic metamaterial with tunable effective density[J]. New Journal of Physics, 2009, 11(11):123010.
[24] Popa B I, Zigoneanu L, Cummer S A. Tunable active acoustic metamaterials[J]. Physical Review B, 2013, 88(2).
[25] Cheng Z, Shi Z. Vibration attenuation properties of periodic rubber concrete panels[J]. Construction & Building Materials, 2014, 50:257-265.
[26] Modinos A. Stefanou N. and Yannopapas V. Applications of the layer-KKR method to photonic crystals [J]. Optics Express, 2001, 8(3): 197-229.
[27] E. Waks, K. Inoue, C. Santori, et al. Secure communication: Quantum cryptography with a photon turnstile [J]. Nature, 2002, 420: 762.